ACS APPLIED MATERIALS & INTERFACES

Research Article

Cite This: ACS Appl. Mater. Interfaces 2019, 11, 13343−13349

www.acsami.org

Half-Pipe Palladium Nanotube-Based Hydrogen Sensor Using a Suspended Nanofiber Scaffold

Minkyu Cho, Jianxiong Zhu, Hyeonggyun Kim, Kyungnam Kang, and Inkyu Park*

Mechanical Engineering and KI for NanoCentry, Korea Advanced Institute of Science and Technology (KAIST), Daejeon 34141, Republic of Korea

Supporting Information

ABSTRACT: A half-pipe palladium nanotube network (H-PdNTN) structure was developed for high-performance hydrogen (H_2) sensor applications. To fabricate the sensor, suspended poly(vinyl alcohol) (PVA) nanofiber bundles were electrospun on a conductive substrate, followed by a palladium (Pd) deposition on top of the PVA nanofiber bundles. Then, Pd-deposited PVA nanofibers were transferred to a host substrate, and the PVA nanofiber templates were selectively removed. Various material analyses confirmed that the PVA nanofibers were successfully dissolved leaving a half-pipe-shaped Pd nanotube network. The fabricated Pd nanotube-based sensors were tested for H_2 responses with different gas concentrations. The 4 nm thick sensor showed the highest response ($\Delta R/R_0$) to H_2 gas. Platinum (Pt) decoration of the sensor showed an improved response speed compared to that of the pristine sensor via the catalytic function of Pt. Additionally, the sensor exhibited good H_2 selectivity against other interfering gases. The H-PdNTN H_2 sensor provides a facile and cost-effective way to fabricate high-performance H_2 sensors.

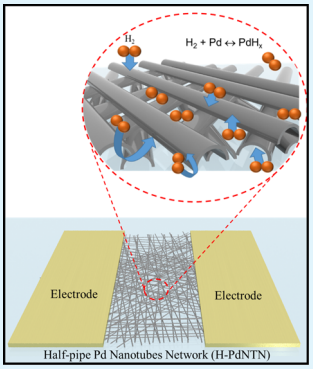

KEYWORDS: *electrospinning, electrospun nanofiber, metal nanostructure, palladium nanotube, hydrogen sensor*

INTRODUCTION

The hydrogen (H_2) economy is rising as a new energy ecosystem for the future. To maintain a stable hydrogen ecosystem, every sector of the system, namely, the source, infrastructure, and fuel storage system, must be secure. The H_2 sensor plays a crucial role in the H_2 economy for early detection of H_2 leakage. There are many types of H_2 sensors: optical fiber type,[1−7] catalytic combustion type,[8−11] chemoresistive type,[12−23] etc. Among various types of chemoresistive-type sensors, Pd-based H_2 sensors have been studied by many researchers because of their advantages, such as simplicity, low power consumption, and fast response. The principle of the Pd-based H_2 sensor is the resistance change by palladium hydride (PdH_x) formation, which is generated from the absorption, dissociation, and diffusion of H_2 into the Pd bulk.[24−26] To enhance the performance of Pd-based H_2 sensors, one of the strategies is to reduce the physical dimension of the sensor such as Pd nanowire for faster response. Various methods to fabricate Pd nanostructure-based H_2 sensors have been reported. A Pd nanowire-based H_2 sensor was demonstrated via an electrophoresis method in which a Pd electrolyte solution was drop-cast onto a poly(methyl methacrylate) channel, followed by applying a current across the channel to grow a Pd nanowire.[27] However, this method suffers from complicated steps for fabricating two electrodes and a 100 nm width channel. Yang suggested a method for growing Pd nanowires laterally using an electrodeposition method.[25,28] In this approach, the width of the nanowire is controlled by the lateral etching of the nickel film underneath the patterned photoresist. However, the wet etching requires stringent control of the etching time and the solution concentrations. To increase the surface area-to-volume ratio of the Pd nanostructure sensors even further, some researchers adopted template methods to realize three-dimensional (3D) Pd nanostructure-based H_2 sensors. Zeng et al. and Cherevko et al. demonstrated Pd nanowire sensors by depositing Pd on an anodized aluminum oxide that showed a good sensing performance.[29,30] Lim et al. demonstrated a method of forming tubular Pd nanostructures by liquid-phased reduction of Pd ions along a ZnO nanowire template with in situ dissolution of the ZnO nanowires.[31]

While various methods to realize nanostructure-based H_2 sensors have been demonstrated, a facile method of fabricating a one-dimensional metal nanostructure has been introduced using electrospinning: Wu et al. demonstrated a method of fabricating transparent gold (Au) electrodes using electrospun nanofibers as templates.[32] Au nanotrough electrodes showed higher transparency and conductivity compared to other existing transparent electrodes. In this work, by adopting that approach, Pd was deposited onto poly(vinyl alcohol) (PVA) nanofibers, followed by a selective removal of the fibers to make half-pipe-shaped Pd nanotubes as a high-performance H_2 sensor. The sensor showed rapid responses to H_2 gas with a response ($\Delta R/R_0$) of 2.1% and a response time ($\tau_{0-80\%}$) of 11 s to 1.8% H_2 concentrations. The effects of thickness and temperature on the sensing performance were also investigated

Received: November 15, 2018
Accepted: March 15, 2019
Published: March 15, 2019

DOI: 10.1021/acsami.8b19848
ACS Appl. Mater. Interfaces 2019, 11, 13343−13349

in the study. Furthermore, metal catalyst effects on the sensor performance were also studied by decorating Pt nanoparticles on the existing sensor structure. There are several advantages to using the electrospinning technology to fabricate Pd nanotube-based H_2 sensors. First, Pd nanotubes can be manufactured at low cost without expensive nanolithography methods. Second, the thickness of a half-pipe palladium nanotube network (H-PdNTN) can be simply controlled by the deposition time of Pd, and this allows the precise control of the nanotube dimensions. Last, it is transferrable onto various substrates, which is not the case with existing bottom-up or top-down Pd nanowire H_2 sensors that are bound to the original substrates(Scheme 1).

Scheme 1. Graphic Illustrations of the Half-Pipe Pd Nanotube Network (H-PdNTN) H_2 Sensor

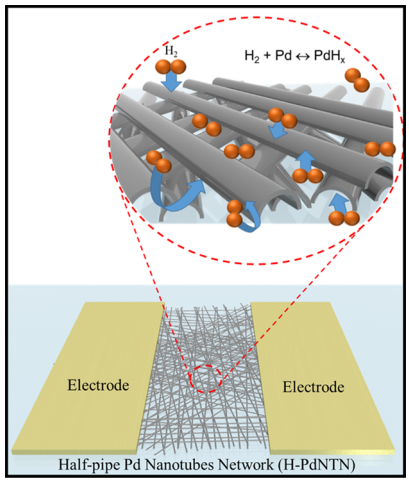

RESULTS AND DISCUSSION

Figure 1a shows the fabrication process of the H-PdNTN H_2 sensor. First of all, PVA nanofibers were electrospun on collecting substrates with holes in the middle, which allowed the PVA nanofiber bundles to be suspended. The collecting substrates with holes also made it possible to transfer H-PdNTN to various substrates. After electrospinning, the suspended PVA nanofibers were mounted in an e-beam evaporation chamber, and a Pd thin film was deposited. Because of the directional deposition of the e-beam evaporation method, only the top half of the PVA nanofibers was covered with the Pd film. Afterward, the Pd-deposited PVA nanofiber bundles were transferred to another substrate, and the PVA nanofibers were selectively removed using organic solvents and therefore only H-PdNTN remained. The details of the fabrication process are explained in the "Methods" section. Photographs of the suspended PVA nanofiber bundles on the collecting substrate are shown in Figures 1b and S1. An optical microscopy image, Figure 1c, and a photograph (inset) of H-PdNTN on a glass substrate indicate its randomly oriented nanotube structure and optical transparency. Figure S2 shows the images of the suspended PVA nanofibers after the Pd deposition and reveals its optical transparency. The transparency was mainly determined by the density of the suspended PVA nanofibers. High-density suspended nanofibers, as shown in Figure S2 (right), block most of the incoming light making it less transparent, whereas less dense suspended nanofibers in Figure S2 (left) have higher

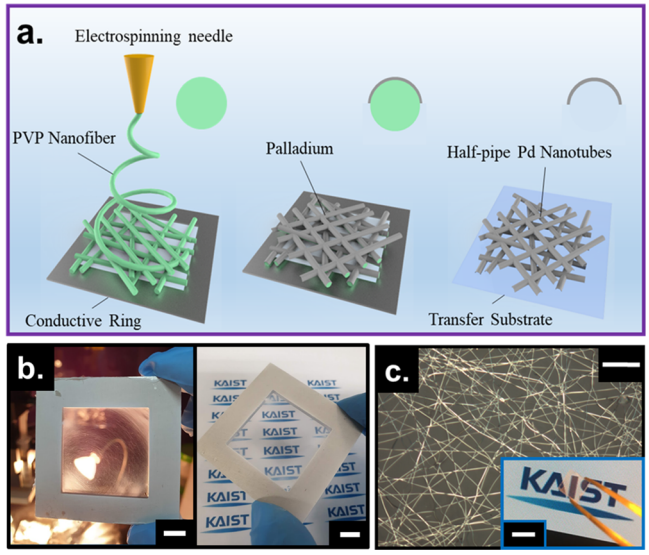

Figure 1. (a) Schematic illustrations of the fabrication process for H-PdNTN, (b) photographic images of PVA nanofibers on metal ring structures (scale bars: 5 mm), (c) optical microscopy and photographic (inset, scale bar: 5 mm) images of electrospun H-PdNTN on a glass substrate (scale bar 30 μm).

transparency, which allows more light to be transmitted. Figure 2a shows the images of electrospun PVA nanofibers (left) and H-PdNTN (right). The tunneling electron microscopy (TEM) image in Figure 2c shows the high-resolution cross-sectional image with a half-pipe shape of 10 nm thick H-PdNT. The high-resolution X-ray photoelectron spectroscopy (XPS) scan of Pd 3d in Figure 2d revealed asymmetric peaks of Pd $3d_{3/2}$ at 340.4 eV and Pd $3d_{5/2}$ at 335.1 eV, respectively, which suggest the existence of palladium oxide (PdO). Energy-dispersive X-ray spectroscopy (EDS) spectra verified the presence of Pd elements of the half-pipe nanotube structures as shown in Figure 2e. Atomic force microscopy (AFM) analysis shows the 20 nm H-PdNT bundles with their morphologies on a quartz substrate in Figure 2f.

Three H-PdNTN sensors with different thicknesses were prepared: 4, 20,, and 50 nm as shown in Figure 3. The thickness of each sensor was controlled by the deposition time and electron beam current. One of the critical factors in fabricating half-pipe Pd nanotubes is that Pd should be able to form continuous films on PVA nanofibers. As a test, 2 nm Pd was deposited on PVA nanofibers and transferred to a quartz substrate. After the PVA nanofibers were dissolved, as shown in Figure S3, no Pd nanotube structures were left on the transferred substrate because no Pd film was formed on the PVA nanofibers with 2 nm deposition. To investigate the thickness dependency of the H_2 sensing performance, gas sensing experiments were performed for each sensor, and the result showed that 4 nm H-PdNTN exhibited the highest response ($\Delta R/R_0$), 2.1−1.8% H_2 concentration, whereas 50 nm H-PdNTN showed the lowest response ($\Delta R/R_0$ = 0.9−1.8% H_2 concentration). This result might be due to the thinner H-PdNTN sensor that had a higher surface area-to-volume ratio. Assuming that H-PdNTN was completely suspended and the surrounding surfaces were fully exposed to H_2, the 4 nm thick H-PdNTN sensor with a curvature radius of 200 nm had a surface area-to-volume ratio about 5 times higher than that of the 20 nm thick H-PdNTN sensor and about 11 times higher than that of the 50 nm thick H-PdNTN.

DOI: 10.1021/acsami.8b19848
ACS Appl. Mater. Interfaces 2019, 11, 13343−13349

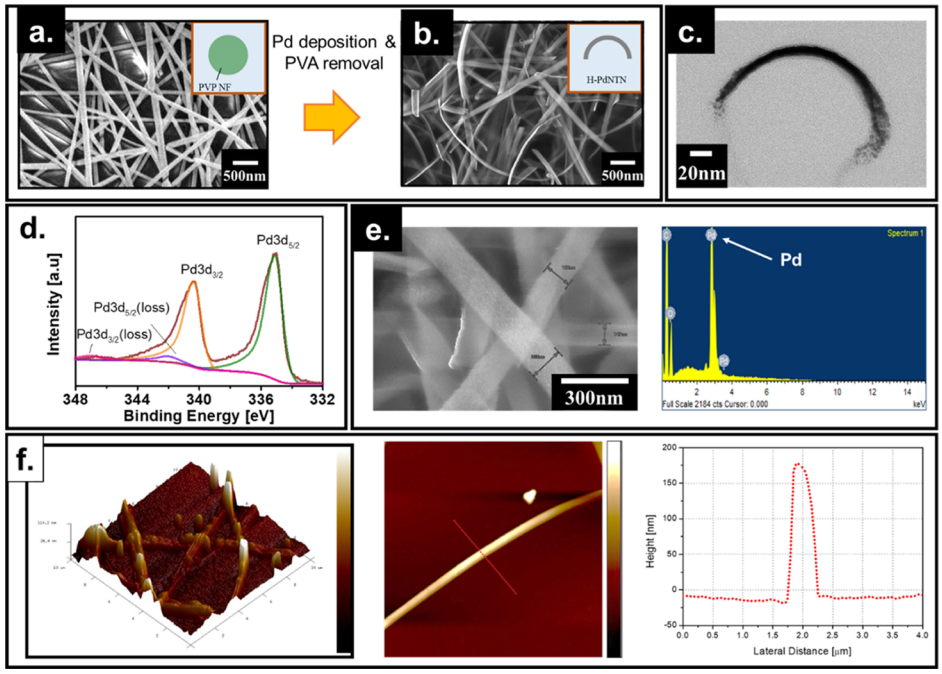

Figure 2. SEM images of the (a) PVA nanofiber network and (b) H-PdNTN. (c) TEM cross-sectional image of H-PDNTN. (d) XPS spectrum of the H-PdNTN sensor. (e) EDS spectrum of the H-PdNTN sample on a glass substrate. (f) AFM scan images of 4 nm H-PdNTN (left) and a single 20 nm H-PdNT (center and right).

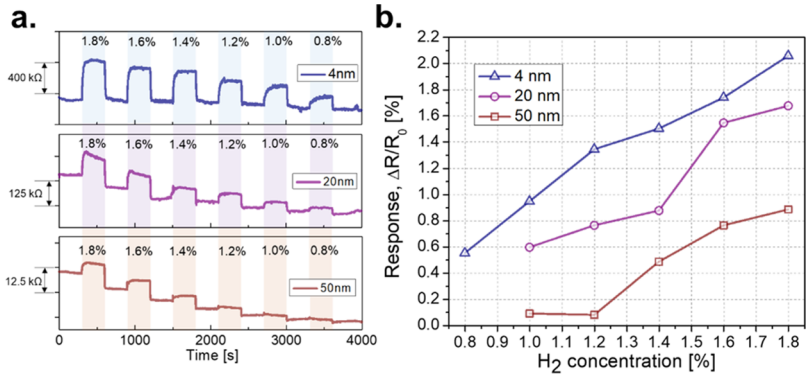

Figure 3. (a) Resistance vs time graph to show H_2 responses of H-PdNTN sensors with different Pd thicknesses to different H_2 concentrations. (b) Response vs H_2 concentrations graph for H-PdNTN sensors with different Pd thicknesses.

However, reducing the Pd thickness did not actually cause a dramatic increase in the response with respect to the increase in surface area-to-volume ratio. In fact, not all the H-PdNTNs were fully suspended in our transferred sensors. In other words, some of the H-PdNTNs might have been bound to the substrate or oriented differently, thereby exposing only a part of the H-PdNTNs to H_2 gas. This is confirmed by scanning electron microscopy (SEM) images in Figure S6. It is difficult to accurately estimate the ratio of suspended H-PdNTN to bound H-PdNTN by existing visual analysis tools. Therefore, the surface area-to-volume ratios of the H-PdNTN structures were calculated and estimated according to different ratios of suspended H-PdNTNs to bound H-PdNTNs as shown in Figure S7. Assuming that the diameter of the PVA nanofiber (two times of the radius of curvature of H-PdNTN) was 200 nm, we found that the surface area-to-volume ratio was affected by the ratio of suspended/bound H-PdNTN. Fully suspended H-PdNTs had the highest surface area-to-volume ratio, whereas fully bound H-PdNTs had the lowest value as shown in Figure S8. Because the structural stability of the thicker H-PdNTs was higher than that of the thinner H-PdNTs, it is a reasonable presumption that the thicker H-PdNTs had a higher proportion of suspended H-PdNTs than the thinner H-PdNTs. The slight enhancement of the sensitivity of the thinner H-PdNTN H_2 sensor as compared to the thicker H-PdNTN H_2 sensor can be explained by this presumption. Therefore, we conjectured that transferring H-PdNTs onto the substrates with more gas accessibility on the backside, such as porous or surface textured substrates, would further enhance the sensing performance by offering a larger effective surface area-to-volume ratio.

To further analyze the effect of the radius of curvature of H-PdNTs on the surface area-to-volume ratio, the surface area-to-volume ratio versus the radius of curvature and the thickness of H-PdNTs was plotted in 3D as shown in Figure S9. Because a variance of the diameter was observed in the electrospun nanofiber in the real experiment, it was important to know whether the variance of the diameters appreciably affects the

DOI: 10.1021/acsami.8b19848
ACS Appl. Mater. Interfaces 2019, 11, 13343−13349

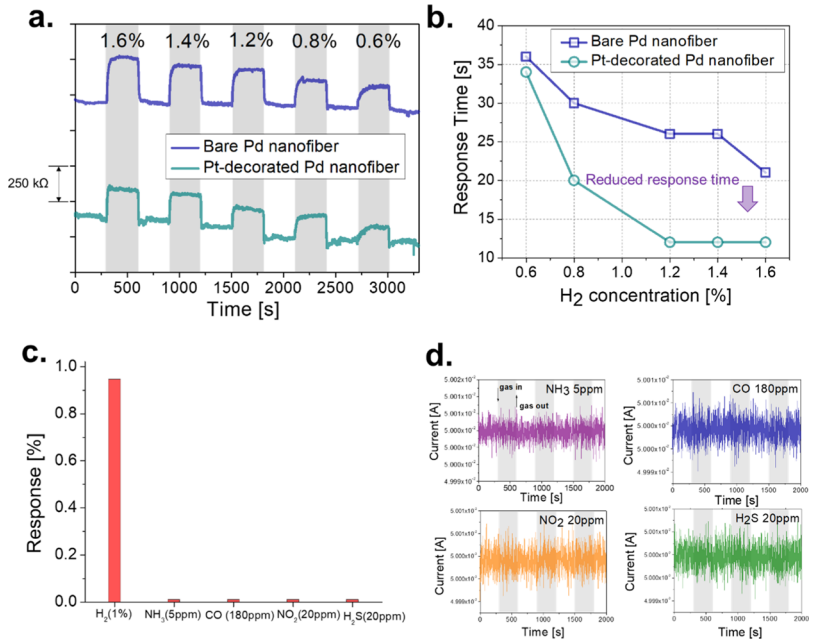

Figure 4. (a) Resistance vs time and (b) response time of the pristine and Pt-decorated H-PdNTN sensors to different H_2 concentrations. (c) Gas responses of H-PdNTN to various test gases: H_2 (1%), NH_3 (5 ppm), CO (180 ppm), NO_2 (20 ppm), and NH_3 (5 ppm). Gas concentrations for the test gases were set on the basis of the PELs by the Occupational Safety and Health Administrations and current available gas sources. (d) Current vs time graph to indicate the response of the H-PdNTN sensor to other interfering gases; it shows little response to other test gases besides H_2.

surface area-to-volume ratio of H-PdNTs. However, there was little effect on the surface area-to-volume ratio by varying the diameter (from 150 to 250 nm) as compared to the change by varying the thickness (from 4 to 50 nm) of PdNTs.

The response and recovery time of the sensor for different Pd thicknesses were measured as shown in Figure S10. For response time, the measurement showed that the response time increased as the thickness of the sensor increased. For recovery time, all tested sensors were less than 15 s in given H_2 concentration ranges (1.2−1.8%), and they increased with larger H_2 concentrations, which was similar to the response time. However, we found no clear relationship between the recovery time and Pd thickness of the sensor. This may have been due to the tested thickness range that was too narrow to see the relationship.

Overall, the response of the H-PdNTN H_2 sensor was not as high as the recent two-dimensional material-based H_2 sensors with heterojunction structures.[35,36] However, it showed relatively fast response/recovery speeds (τ_{0-80} = 12 s and τ_{100-20} = 18 s for 4 nm H-PdNTN to 1.8% H_2) in given concentration ranges (1−1.8%) as shown in Figure S10.

The limit of detection (LOD) of the sensor was measured using a linear approximation of the graph as shown in Figure S11. The LOD of the sensor was about 314 ppm. The LOD of the sensor was low enough to detect H_2 concentrations considering that the lower flammability limit of H_2 is about 4%.

To understand the temperature effects of the sensor, the H-PdNTN H_2 sensors were tested with different H_2 concentrations at three different temperatures: 296, 316, and 336 K as shown in Figure S12a. The response at room temperature (296 K) showed the highest value while that at 336 K showed the lowest value. As the temperature increased, absorbed H_2 molecules gained enough kinetic energy to desorb from the Pd surface. According to Sievert's law, H_2 solubility is proportional to the inverse of the temperature[33]

$$C_H = K_H P_{H_2}^{1/2} \quad (1)$$

where C_H is the H_2 content on Pd expressed as an atomic ratio (H/Pd), P_{H_2} is the partial pressure of H_2, and K_H is Sievert's constant, which is formulated by the following equation

$$K_H = A + \frac{B}{T} \quad (2)$$

where A and B are constants and T is the absolute temperature. It was confirmed that our measurement result, a reduced H_2 response versus the square root of the H_2 partial pressure at a higher temperature, in Figure S12 satisfies Sievert's law.

To observe the effect of platinum (Pt) decoration on the sensing performance of the H-PdNTN H_2 sensor, Pt was sputtered on a pristine H-PdNTN sensor, and the changes in H_2 sensing performances were monitored through material analysis and gas sensing measurements. We reasoned that if Pt fully covered H-PdNTN, it could result in the decreased sensitivity because the deposited Pt would block the Pd reaction sites. For comparison, the XPS scan of the H-PdNTN sample after Pt sputtering was also performed as shown in Figure S13, which clearly depicts the presence of double Pt peaks: Pt $4f_{5/2}$ at 75.5 eV and Pt $4f_{7/2}$ at 71.3 eV on the H-PdNTN sensor after the sputtering. For H_2 sensing measurement, pristine and Pt-coated H-PdNTNs were mounted in a gas chamber with a constant flow rate of 500 sccm throughout the experiment. As shown in Figure 4a,b, the gas sensing test revealed that the resistance decreased, and there was a shorter response time (11 s vs 21 s @ 1.8% H_2 concentration) after Pt sputtering. The recovery speed also increased after Pt decoration as shown in Figure S14. The gas sensing experiment results confirmed that Pt worked as a catalyst to accelerate the reaction between Pd and H_2 over all the tested concentration range. However, the sensitivity result showed that the Pt-coated H-PdNTN sensor had lower sensitivity compared to

DOI: 10.1021/acsami.8b19848
ACS Appl. Mater. Interfaces 2019, 11, 13343−13349

the pristine H-PdNTN sensor, and this may have been due to the sputtered Pt that hindered the formation of PdH_x by partially blocking Pd reaction sites. A study conducted by another group claimed that the water formation by the surface Pt was responsible for the decreased sensitivity.[34] Nevertheless, our experimental result suggested that there may be a trade-off between the sensitivity and the response time for different Pt loading amounts. Further investigations will be carried out in the future to find the optimal Pt deposition condition.

To investigate the influence of humidity on the sensor performance, the sensor was tested in high humidity. In high humidity, water molecules in the air were condensed on the surface of the sensor, which hindered the reaction of H_2 gas to Pd. Figure S15 reveals that there was about a 10−12% decreased response in 60% relative humidity conditions compared to the response in dry conditions. The cyclic and durability test of the sensor was performed[37] as shown in Figure S16. After 6 days, there was about a 34% decreased response.

Because the ideal H_2 sensor should only respond to H_2 gas among many other gases, we characterized the selectivity of H-PdNTN sensors against other gases as shown in Figure 4c,d. Other gases for the selectivity test included NO_2, NH_3, CO, and H_2S. The permissible exposure limits (PELs) set by the Occupational Safety and Health Administration (OSHA) for the test gases were 5 ppm for NO_2, 10 ppm for H_2S, 50 ppm for CO, and 50 ppm for NH_3. The tested concentration for H_2 for comparison was much higher than the concentration range for other test gases, but considering the lower flammability limit of H_2 (4%), our gas exhibited good selectivity over the other test gases in practical applications.

CONCLUSIONS

In conclusion, we demonstrated an H-PdNTN H_2 sensor using electrospinning and e-beam evaporation, followed by the transfer to another substrate. With this method, half-pipe-shaped Pd nanostructures were formed at low cost, and the tube thickness could be easily controlled by the e-beam evaporation process. Various material analyses revealed the formation of H-PdNTN with its structural and chemical characteristics. The H_2 gas sensing test revealed that reducing the thickness of the H-PdNTN H_2 sensor is the main factor to improve the H_2 sensing characteristics, namely, H_2 sensitivity and response time. Our results and hypothesis on the thickness dependency on the H_2 response were confirmed by calculating the surface area-to-volume ratio of H-PdNTN for different thicknesses. The effect of the Pt catalyst on the H_2 sensing performance was also investigated, and our experiment indicated that the Pt-decorated H-PdNTN sensor had a quicker response than that of the pristine H-PdNTN sensor by almost 2-fold. The sensor followed H_2 absorption characteristics on Pd according to Sievert's law, resulting in concentration and temperature dependence. The sensor also showed an excellent H_2 selectivity among other gases, NH_3, NO_2, H_2S, and CO. The proposed method does not require expensive lithography equipment nor stringent control of chemical etching. This method will be useful for low-cost, facile nanostructure-integrated gas sensor fabrication because of its simple manufacturing process and applicability to areas such as H_2 storage and biofuel cells, which would benefit from nanostructures with a high surface area-to-volume ratio.

METHODS

Electrospinning Suspended PVA Nanofiber Bundles. Ten wt % PVA solution (Sigma-Aldrich, M_w = 13 000 000) mixed with deionized water was prepared by magnetic stirring at 80 °C. Then, the PVA solution was loaded into a 5 mL syringe with a 24 G metal needle attached. For electrospinning, an 80 mL/s pulling rate was used and 19 kV was applied to the metal needle for continuous jetting of PVA nanofibers. The distance between the needle tip and the collecting substrate was about 15 cm. Various collecting substrates with different hole sizes were prepared by CNC machining of aluminum plates. The dimensions of the holes in the collecting substrates were varied between 1 and 3 cm in length/width. During electrospinning, jetted PVA nanofibers were collected in suspended form on the hole of the collecting substrate. Changing the geometries of the holes in the collecting substrates and the electrospinning time determined the orientation and the areal density of the suspended PVA nanofiber bundles.

Deposition of Palladium, H-PdNTN Transfer, and Electrode Formation. The suspended PVA nanofiber bundles were placed in an e-beam vacuum chamber under a pressure of $\sim 2 \times 10^{-6}$ Torr, and the thickness of the deposited Pd was monitored with a quartz crystal monitor during the deposition. Throughout the deposition process, the temperature inside the chamber was kept under 60 °C because a higher deposition temperature damages the PVA nanofiber bundles. After the Pd deposition, the Pd-deposited PVA nanofiber bundles were transferred to a glass substrate and the PVA nanofibers were dissolved with organic solvents leaving half-pipe-shaped Pd nanotube bundles. For stable electrical connection, two methods were used to make sensor electrodes after the H-PdNTN transfer. The first method was to use a silver paste. In the second method, a tungsten wire with a 50 μm diameter was placed on top of the transferred H-PdNTN, and Au was selectively deposited as shown in Figure S4.

Decoration of Platinum. Platinum was sputtered with a 3 mA current under 0.1 Torr. In these conditions, 1 nm of Pt was deposited on existing Pd nanotubes. AFM data showed that the sputtered Pt had an average roughness of 0.1 nm in root mean square. Resistance measurement of the sputtered Pt film verified that the percolation threshold had not been reached with the given deposition condition.

Gas Sensing Test. The H-PdNTN H_2 sensor was tested inside a sealed chamber with gas inlets/outlets. There was a probing station inside the gas chamber, and the voltage across the sensor was applied by a current source, while the current change of the sensor was monitored in real time. A gas test was performed in a dry air environment, and the gas flows were controlled by mass flow controllers that were connected to a computer with a LabVIEW interface. The total gas flow rate was kept at 500 sccm. The H_2 test was conducted in synthetic air base by mixing N_2 and O_2 in a 4:1 ratio. For the temperature test, a hot plate with a thermocouple was placed underneath the sample and left for 30 min before each gas test for even temperature distribution throughout the test sample.

ASSOCIATED CONTENT

Supporting Information

The Supporting Information is available free of charge on the ACS Publications website at DOI: 10.1021/acsami.8b19848.

Photographic and optical microscopic images after electrospinning PVA nanofibers on a rectangular metal ring (left) and a square metal ring (right); photographic images of suspended low-density (electrospun for 5 min, left) and high-density (electrospun for 30 min, right) suspended PVA nanofiber mat after Pd deposition; optical microscopy images of 2 nm deposited Pd/PVA nanofiber structures on a quartz substrate: before and after PVA nanofiber dissolution; current versus voltage graph of a 4 nm thick H-PdNTN sensor; optical microscopy image of the H-PdNTN H_2 sensor with Au electrode deposition; tilted-view SEM images of 20 nm

DOI: 10.1021/acsami.8b19848
ACS Appl. Mater. Interfaces 2019, 11, 13343−13349

(top) and 50 nm (bottom) H-PdNTN on a quartz substrate; calculations to estimate the surface area-to-volume ratio of the H-PdNTN structure; surface area-to-volume ratio versus the thickness of H-PdNT for different suspended/bound H-PdNTN ratios and PVA diameters; surface area-to-volume ratio versus the H-PdNT wall thickness and the diameter of nanofibers; response and recovery time of the H-PdNTNs sensor with different thicknesses: 4, 20, and 50 nm; resistance versus time to show H_2 responses of H-PdNTN sensors for different temperatures and H_2 concentrations and response versus H_2 concentrations graph for different temperatures; XPS spectrum of pristine and Pt-decorated H-PdNTN sensors; recovery time of the pristine and Pt-decorated H-PdNTN sensors to different H_2 concentrations; resistance versus time graphs in different humidity conditions; and cyclic and durability test of the sensor (PDF)

AUTHOR INFORMATION

Corresponding Author

*E-mail: inkyu@kaist.ac.kr.

ORCID

Minkyu Cho: 0000-0002-0006-2063

Inkyu Park: 0000-0001-5761-7739

Notes

The authors declare no competing financial interest.

ACKNOWLEDGMENTS

This work was supported by the National Research Foundation of Korea (NRF) grant funded by the Korea government (MSIT) (nos. 2018R1C1B600338, 2018R1A2B2004910, and 2015R1A5A1037668).

REFERENCES

(1) Tabib-Azar, M.; Sutapun, B.; Petrick, R.; Kazemi, A. Highly Sensitive Hydrogen Sensors Using Palladium Coated Fiber Optics with Exposed Cores and Evanescent Field Interactions. *Sens. Actuators, B* **1999**, *56*, 158−163.

(2) Butler, M. A. Micromirror Optical-Fiber Hydrogen Sensor. *Sens. Actuators, B* **1994**, *22*, 155−163.

(3) Villatoro, J.; Luna-Moreno, D.; Monzón-Hernández, D. Optical Fiber Hydrogen Sensor for Concentrations Below The Lower Explosive Limit. *Sens. Actuators, B* **2005**, *110*, 23−27.

(4) Perrotton, C.; Westerwaal, R. J.; Javahiraly, N.; Slaman, M.; Schreuders, H.; Dam, B.; Meyrueis, P. A Reliable, Sensitive and Fast Optical Fiber Hydrogen Sensor Based on Surface Plasmon Resonance. *Opt. Express* **2013**, *21*, 382−390.

(5) Luna-Moreno, D.; Monzón-Hernández, D.; Villatoro, J.; Badenes, G. Optical fiber hydrogen sensor based on core diameter mismatch and annealed Pd-Au thin films. *Sens. Actuator, B* **2007**, *125*, 66−71.

(6) Okazaki, S.; Nakagawa, H.; Asakura, S.; Tomiuchi, Y.; Tsuji, N.; Murayama, H.; Washiya, M. Sensing Characteristics of an Optical Fiber Sensor for Hydrogen Leak. *Sens. Actuators, B* **2003**, *93*, 142−147.

(7) Bévenot, X.; Trouillet, A.; Veillas, C.; Gagnaire, H.; Clément, M. Hydrogen Leak Detection Using an Optical Fibre Sensor for Aerospace Applications. *Sens. Actuators, B* **2000**, *67*, 57−67.

(8) Lee, E.-B.; Hwang, I.-S.; Cha, J.-H.; Lee, H.-J.; Lee, W.-B.; Pak, J. J.; Lee, J.-H.; Ju, B.-K. Micromachined Catalytic Combustible Hydrogen Gas Sensor. *Sens. Actuators, B* **2011**, *153*, 392−397.

(9) Park, N.-H.; Akamatsu, T.; Itoh, T.; Izu, N.; Shin, W. Calorimetric Thermoelectric Gas Sensor for the Detection of Hydrogen, Methane and Mixed Gases. *Sensors* **2014**, *14*, 8350.

(10) Nishibori, M.; Shin, W.; Houlet, L. F.; Tajima, K.; Itoh, T.; Izu, N.; Murayama, N.; Matsubara, I. New Structural Design of Micro-Thermoelectric Sensor for Wide Range Hydrogen Detection. *J. Ceram, Soc. Jpn.* **2006**, *114*, 853−856.

(11) Jones, M. G.; Nevell, T. G. The Detection of Hydrogen Using Catalytic Flammable Gas Sensors. *Sens. Actuators* **1989**, *16*, 215−224.

(12) Lange, U.; Hirsch, T.; Mirsky, V. M.; Wolfbeis, O. S. Hydrogen sensor based on a graphene - palladium nanocomposite. *Electrochim. Acta* **2011**, *56*, 3707−3712.

(13) Mubeen, S.; Zhang, T.; Yoo, B.; Deshusses, M. A.; Myung, N. V. Palladium Nanoparticles Decorated Single-Walled Carbon Nanotube Hydrogen Sensor. *J. Phys. Chem. C* **2007**, *111*, 6321−6327.

(14) Ahn, J.-H.; Yun, J.; Choi, Y.-K.; Park, I. Palladium Nanoparticle Decorated Silicon Nanowire Field-Effect Transistor with Side-Gates for Hydrogen Gas Detection. *Appl. Phys. Lett.* **2014**, *104*, 013508.

(15) Gao, M.; Cho, M.; Han, H.-J.; Jung, Y. S.; Park, I. Palladium-Decorated Silicon Nanomesh Fabricated by Nanosphere Lithography for High Performance, Room Temperature Hydrogen Sensing. *Small* **2018**, *14*, 1703691.

(16) Cho, M.; Yun, J.; Kwon, D.; Kim, K.; Park, I. High-Sensitivity and Low-Power Flexible Schottky Hydrogen Sensor Based on Silicon Nanomembrane. *ACS Appl. Mater. Interfaces* **2018**, *10*, 12870−12877.

(17) Shukla, S.; Seal, S.; Ludwig, L.; Parish, C. Nanocrystalline Indium Oxide-Doped Tin Oxide Thin Film as Low Temperature Hydrogen Sensor. *Sens. Actuators, B* **2004**, *97*, 256−265.

(18) Varghese, O. K.; Gong, D.; Paulose, M.; Ong, K. G.; Grimes, C. A. Hydrogen Sensing Using Titania Nanotubes. *Sens. Actuators, B* **2003**, *93*, 338−344.

(19) Şennik, E.; Çolak, Z.; Kılınç, N.; Öztürk, Z. Z. Synthesis of Highly-Ordered TiO_2 Nanotubes for a Hydrogen Sensor. *Int. J. Hydrog. Energy* **2010**, *35*, 4420−4427.

(20) Wang, H. T.; Kang, B. S.; Ren, F.; Tien, L. C.; Sadik, P. W.; Norton, D. P.; Pearton, S. J.; Lin, J. Hydrogen-Selective Sensing at Room Temperature with ZnO Nanorods. *Appl. Phys. Lett.* **2005**, *86*, 243503.

(21) Basu, S.; Dutta, A. Modified Heterojunction based on Zinc Oxide Thin Film for Hydrogen Gas-Sensor Application. *Sens. Actuators, B* **1994**, *22*, 83−87.

(22) Lupan, O.; Chai, G.; Chow, L. Novel Hydrogen Gas Sensor based on Single ZnO Nanorod. *Microelectron. Eng.* **2008**, *85*, 2220−2225.

(23) Tien, L. C.; Sadik, P. W.; Norton, D. P.; Voss, L. F.; Pearton, S. J.; Wang, H. T.; Kang, B. S.; Ren, F.; Jun, J.; Lin, J. Hydrogen Sensing at Room Temperature with Pt-Coated ZnO Thin films and Nanorods. *Appl. Phys. Lett.* **2005**, *87*, 222106.

(24) Offermans, P.; Tong, H. D.; van Rijn, C. J. M.; Merken, P.; Brongersma, S. H.; Crego-Calama, M. Ultralow-Power Hydrogen Sensing with Single Palladium Nanowires. *Appl. Phys. Lett.* **2009**, *94*, 223110.

(25) Yang, F.; Taggart, D. K.; Penner, R. M. Joule Heating a Palladium Nanowire Sensor for Accelerated Response and Recovery to Hydrogen Gas. *Small* **2010**, *6*, 1422−1429.

(26) Atashbar, M. Z.; Banerji, D.; Singamaneni, S. Room-Temperature Hydrogen Sensor based on Palladium Nanowires. *IEEE Sens. J.* **2005**, *5*, 792−797.

(27) Hu, Y.; Perello, D.; Mushtaq, U.; Yun, M. A Single Palladium Nanowire Via Electrophoresis Deposition Used as a Ultrasensitive Hydrogen Sensor. *IEEE Trans. Nanotechnol.* **2008**, *7*, 693−699.

(28) Yang, F.; Taggart, D. K.; Penner, R. M. Fast, Sensitive Hydrogen Gas Detection Using Single Palladium Nanowires That Resist Fracture. *Nano Lett.* **2009**, *9*, 2177−2182.

(29) Zeng, X. Q.; Latimer, M. L.; Xiao, Z. L.; Panuganti, S.; Welp, U.; Kwok, W. K.; Xu, T. Hydrogen Gas Sensing with Networks of Ultrasmall Palladium Nanowires Formed on Filtration Membranes. *Nano Lett.* **2011**, *11*, 262−268.

DOI: 10.1021/acsami.8b19848
ACS Appl. Mater. Interfaces 2019, 11, 13343−13349

(30) Cherevko, S.; Kulyk, N.; Fu, J.; Chung, C.-H. Hydrogen Sensing Performance of Electrodeposited Conoidal Palladium Nanowire and Nanotube Arrays. *Sens. Actuators, B* **2009**, *136*, 388−391.
(31) Lim, M. A.; Kim, D. H.; Park, C.-O.; Lee, Y. W.; Han, S. W.; Li, Z.; Williams, R. S.; Park, I. A New Route toward Ultrasensitive, Flexible Chemical Sensors: Metal Nanotubes by Wet-Chemical Synthesis along Sacrificial Nanowire Templates. *ACS Nano* **2012**, *6*, 598−608.
(32) Wu, H.; Kong, D.; Ruan, Z.; Hsu, P.-C.; Wang, S.; Yu, Z.; Carney, T. J.; Hu, L.; Fan, S.; Cui, Y. A Transparent Electrode based on a Metal Nanotrough Network. *Nat. Nanotechnol.* **2013**, *8*, 421−425.
(33) Yamanaka, S.; Higuchi, K.; Miyake, M. Hydrogen Solubility in Zirconium Alloys. *J. Alloys Compd.* **1995**, *231*, 503−507.
(34) Li, X.; Liu, Y.; Hemminger, J. C.; Penner, R. M. Catalytically Activated Palladium@Platinum Nanowires for Accelerated Hydrogen Gas Detection. *ACS Nano* **2015**, *9*, 3215−3225.
(35) Hao, L.; Liu, H.; Xu, H.; Dong, S.; Du, Y.; Wu, Y.; Zeng, H.; Zhu, J.; Liu, Y. Flexible Pd-WS_2/Si heterojunction sensors for highly sensitive detection of hydrogen at room temperature. *Sens. and Actuators, B* **2019**, *283*, 740−748.
(36) Hao, L.; Liu, Y.; Du, Y.; Chen, Z.; Han, Z.; Xu, Z.; Zhu, J. Highly Enhanced H_2 Sensing Performance of Few-Layer MoS_2/SiO_2/Si Heterojunctions by Surface Decoration of Pd Nanoparticles. *Nanoscale Res. Lett.* **2017**, *12*, 567.
(37) Mourya, S.; Kumar, A.; Jaiswal, J.; Malik, G.; Kumar, B.; Chandra, R. Development of Pd-Pt functionalized high performance H_2 gas sensor based on silicon carbide coated porous silicon for extreme environment applications. *Sens. Actuators, B* **2019**, *283*, 373−383.

DOI: 10.1021/acsami.8b19848
ACS Appl. Mater. Interfaces 2019, 11, 13343−13349